Journal of Nuclear Materials xxx (xxxx) 153573

Contents lists available at ScienceDirect

Journal of Nuclear Materials

journal homepage: www.elsevier.com/locate/jnucmat

Engineering defect energy landscape of CoCrFeNi high-entropy alloys by the introduction of additional dopants

Shijun Zhao [a,*], Yanwen Zhang [b], William J. Weber [c]

[a] Department of Mechanical Engineering, City University of Hong Kong, Hong Kong
[b] Materials Science and Technology Division, Oak Ridge National Laboratory, Oak Ridge, TN, United State of America
[c] Department of Materials Science and Engineering, University of Tennessee, Knoxville, TN, United State of America

ARTICLE INFO

Article history:
Received 8 November 2021
Received in revised form 26 January 2022
Accepted 28 January 2022

ABSTRACT

The concept of high-entropy alloys (HEAs) focusing on tuning the overall chemical complexity represents a novel alloy design strategy. In contrast, alloying of a metallic matrix with minor doping elements with limited and localized tunability has been a common practice to improve material performance. Combining the idea of globally engineering defect energy landscape in HEAs and the localized doping strategy in dilute alloys, in this work, we explore doping effects of minor elements in a HEA matrix to further enhance the overall and localized chemical tunability, aiming to improve its irradiation resistance. Specifically, we study the influence of minor Al, Cu, Ti, and Pd substitutional doping elements on defect energetics in a CoCrFeNi model HEA based on density-functional theory (DFT) calculations. The DFT results indicate that the formation and migration energies of vacancies can be strongly influenced when a dopant is introduced at the first nearest neighbor shells around a vacancy. On the other hand, interstitial energetics are only slightly affected. Among the four elements, Ti and Pd generally decrease vacancy formation energies and increase vacancy migration energies more significantly than Al and Cu. The doping effects become more pronounced when the concentration of the substitutional dopants increases. Based on the energy distributions obtained from DFT, we build a kinetic Monte Carlo (kMC) model to assess the impact of dopants on vacancy-mediated diffusivity in the doped HEAs. Our results suggest that Ti and Pd can lower the tracer diffusivity in the considered HEAs and act as trapping sites, whereas Cu may enhance the atomic transport. This work indicates that substitutional doping in HEAs is an effective strategy in metallurgy to further tune the defect and transport properties of complex alloys.

1. Introduction

Alloy development is one of the critical stimulations that advance human civilization. Traditionally, alloys are produced by adding a small number of impurities into a matrix, which is usually one or more metal species or non-metals. The as-doped elements dopants can reside in either interstitial or substitutional positions, which induce local lattice distortion and affect the motion of various defects (e.g., dislocations), leading to enhanced mechanical properties and improved irradiation resistance. The properties of these dilute alloys rely heavily on the matrix, and different alloy systems are developed in this way, such as extensively studied Ni-based alloys, Co-based alloys, and Mg-based alloys [1]. Since the principal elements in these alloys are fixed, the performance improvement by incorporating minor components is somewhat limited.

In contrast to traditional alloys, the recent development of multi-principal elemental alloys, e.g., high-entropy alloys (HEAs) represents a novel alloy design strategy [2–6]. HEAs are composed of multiple elements at or near equiatomic ratio that form single-phase solid solutions on a simple crystal lattice, i.e., face-centered cubic (*fcc*), body-centered cubic (*bcc*), or hexagonal close-packed (*hcp*). Different from traditional alloys that focus on an edge or corner of the phase diagram, the alloy compositions of HEAs locate around the center of the phase diagram [7,8]. Depending on the composition, it has been demonstrated that HEAs can exhibit excellent mechanical properties [9,10], good corrosion resistance [11,12], and radiation resistance [6,13–16]. These properties lead to a new alloy design concept by tuning chemical complexity [6,17–19], making HEAs strong candidates as structural materials in next-generation nuclear reactors. Indeed, great efforts have been devoted to investigating the radiation performance of various HEAs in order to exploit the link between the extreme chemical disorder and their radiation resistance [6,13,15,20–27].

* Corresponding author.
E-mail address: shijzhao@cityu.edu.hk (S. Zhao).

https://doi.org/10.1016/j.jnucmat.2022.153573
0022-3115/

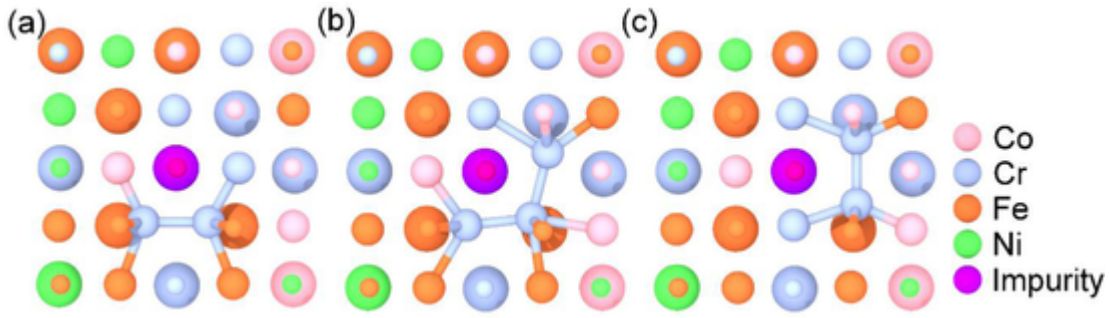

Fig. 1. Atomic configurations used to calculate formation and migration energies of an interstitial dumbbell in doped CoCrFeNi. The purple balls represent impurities. The initial and final states in (a) and (c) are both [100] dumbbells, while the configuration in (b) is the saddle structure.

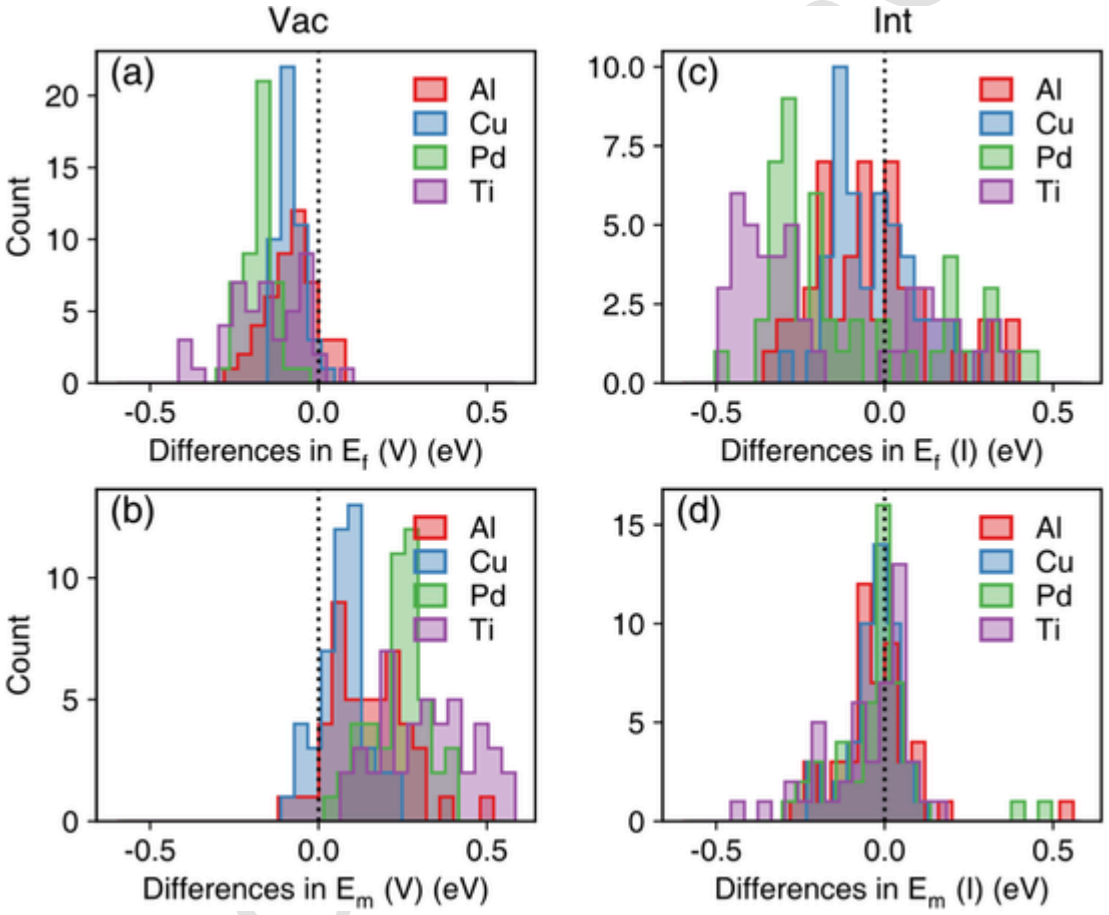

Fig. 2. Influences of doping elements, Al, Cu, Pd, and Ti on the formation and migration energies of vacancies and interstitials in CoCrFeNi.

At the fundamental level, irradiation tolerance of HEAs is closely related to the defect energy landscape under the influence of extreme disorder. Experiments show that defect dynamics in HEAs are strongly suppressed, resulting in their good phase stability with limited solute depletion or enrichment at grain boundaries [25]. Besides, defect (dislocation loops and vacancy clusters) size and void swelling in HEAs are reduced at different irradiation conditions [21,26]. Because of chemical disorder, there are local traps in the energy landscape so that mobile defects will spend most of their time, which contributes to delayed defect evolution observed experimentally. Therefore, the knowledge of defect energetics is vital for the understanding of the irradiation response of HEAs.

As HEAs possess extraordinary properties compared to pure metals, it is expected that further performance improvement may be achieved by doping low-concentration impurities into a HEA matrix by combining the idea of traditional and concentrated alloys [6]. The intrinsic chemical disorder in HEAs produces various defect traps [28]. Built upon such a rough landscape, the presence of a small number of impurities may enhance the atomic-level heterogeneity and induce extra deep traps, which allow additional control of defect behavior and ultimately tailor defect dynamics and irradiation performance.

The irradiation response properties of a few minor element doped-HEAs have been reported in the literature. Xia *et al.* [26,29,30] and Yang *et al.* [31] studied the structural damage and chemical segregation in Al–doped NiCoFeCr under 3 MeV Au ions at different temperatures and different doses. They found that this alloy system exhibits great phase stability without significant phase transformation and decomposition. Chen *et al.* [32] radiated $NiCoFeCrTi_{0.2}$ with 275 keV He^+ at 400°C and found that the faulted loops have a much large size, whereas the perfect loops were rarely detected, which is interpreted by its low

Table 1
Average variations of defect energies (in eV) when one lattice atom in the 1nn shell of the defect is replaced by the impurity.

	Al	Cu	Pd	Ti
E_f(V)	-0.10	-0.08	-0.18	-0.16
E_m(V)	0.13	0.06	0.24	0.34
E_f(I)	-0.01	0.00	-0.10	-0.19
E_m(I)	-0.01	-0.02	-0.02	-0.06

stacking fault energy. In the CoCrFeNi HEA with 0.2 molar ratio of Al/Cu/Ti addition [33], it was found that such minor doping elements have a significant influence on the size and number density distributions of irradiation-induced He bubbles. Besides substitutional dopants as listed above, interstitial doping is also applied to tune vacancy diffusion in the equiatomic FeMnNiCoCr HEAs [34]. The above results indicate that doping is an effective strategy to tune the irradiation responses of HEAs. However, systematic studies still need to be performed to further clarify the effects of doping elements.

In these widely-studied HEAs composed of 3*d* transition metals, it has been proved that the 3*d* electron configurations, especially the valence electron counts, play dominant roles in determining defect energetics and irradiation response [6,35,36]. Tuning *d* electrons through the incorporation of minor dopants is, therefore, a promising strategy to engineer the defect energy landscape of HEAs [19]. In this work, we study the influence of minor substitutional doping elements, including Al, Cu, Pd, and Ti, on defect properties in a CoCrFeNi HEA using density-functional theory (DFT) calculations. These four doping elements are chosen due to their distinct electron configurations and atomic size, as well as their experimental relevance. DFT calculations are carried out to probe changes in defect energies at different local environments when dopant elements are introduced in the first nearest neighbor shell (1nn) of the considered defect, i.e., single vacancy and interstitial. Based on obtained defect energy distributions, kinetic Monte Carlo (kMC) simulations are set up to obtain atomic transport properties without and with doping. Our results demonstrate that doping has a significant influence on defect energetics and mass transport in HEAs. By choosing suitable doping elements, the irradiation performance of HEAs can be tailored accordingly.

2. Method

2.1. DFT calculations

Simulations were performed using the projector augmented wave (PAW) method [37] as implemented in the VASP code [38]. Exchange and correlation were treated in the Perdew-Burke-Ernzerhof [39] form. The energy cutoff of plane waves was 300 eV, and the total energy convergence criterion was set to 10^{-4} eV. Defect energies calculations were carried out in a cubic $4 \times 4 \times 4$ *fcc* supercell containing 256 atoms. Special quasirandom structures (SQS) were used to model disordered structures, which were constructed by optimizing the Warren-Cowley short-range order parameters [40,41] using a simulated annealing algorithm [42]. The volume was frozen at the optimal value, and only atomic positions were fully relaxed until all forces were less than 0.01 eV/Å in defect simulations. Spin polarization was considered throughout all simulations. We mainly consider the ferromagnetic state of this alloy, and the initial magnetic moments for different elements are assigned based on our previous calculations [42].

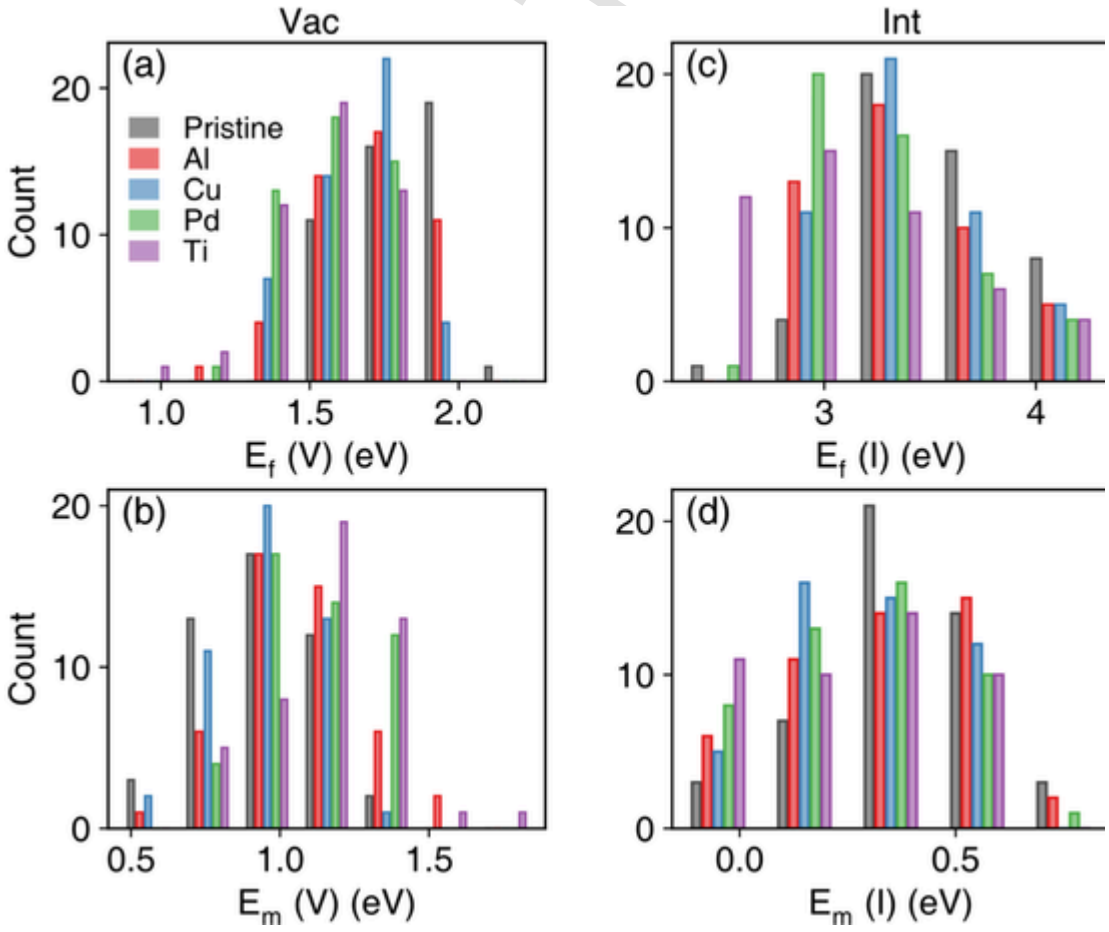

Fig. 3. Distribution of defect energies in pristine CoCrFeNi and minor elements doped ones.

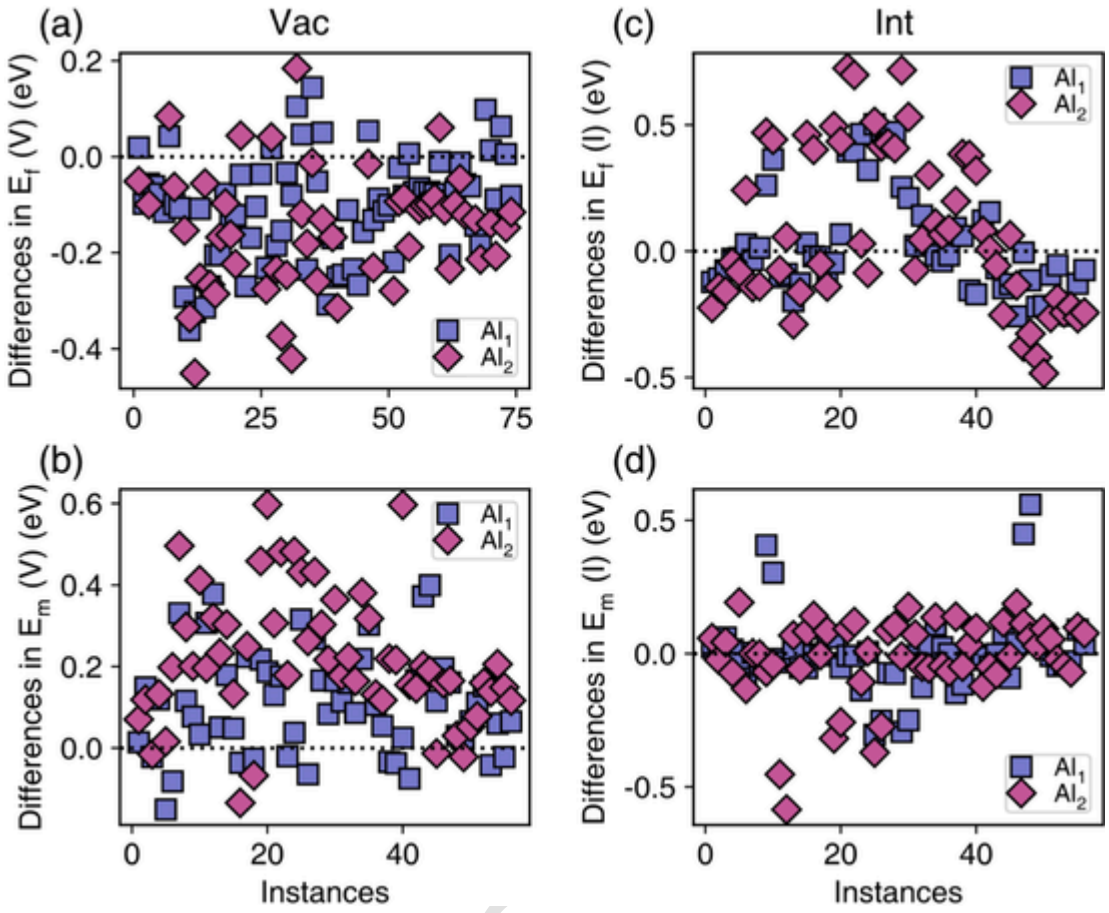

Fig. 4. Effects of increasing the concentration of Al dopants in the 1nn shell around the defect on the differences of defect energies E_f(V), E_m(V), E_f(I), and E_m(I). All energies are shown with respect to those in the pristine CoCrFeNi.

Defect energies were calculated following our previous methodology [35,43]. The formation energies of a vacancy or an interstitial in the pristine HEA is defined by

$$E_f = E_d^{HEA} - E_0^{HEA} \pm \mu_d, \tag{1}$$

where E_d^{HEA} and E_0^{HEA} are the energies of the HEA with and without a defect, respectively, and μ_d is the elemental chemical potential of the element that is removed or added to create the defect. The values of μ_d in the considered CoCrFeNi HEA have been listed in our previous study [35]. In the doped HEA, the formation energy becomes

$$E_f^d = E_d^{dHEA} - E_0^{dHEA} \pm \mu_d, \tag{2}$$

where E_d^{dHEA} and E_0^{dHEA} are the energies of the doped-HEA with and without a defect, respectively. The energy differences in these two formulae can be used to measure the influence of the dopant on defect properties in the HEA,

$$\Delta E_f = E_f^d - E_f. \tag{3}$$

In dilute alloys, the interactions between solute and defects are usually quantified by binding energy. By definition, the indirect method [44] to calculate the binding energy is identical to ΔE_f as defined above. Therefore, ΔE_f is used in this work to characterize the interaction between dopant and defect in the considered HEA.

Following our previous study [35], migration energies of defects were obtained by directly optimizing the saddle structure, which is taken as the midpoint for a vacancy or interstitial dumbbell transition path. The obtained energy differences from the saddle and initial structures are energy barriers, i.e., $E_m = E_s - E_d$. Due to computational cost, we selected typical configurations for defect calculations by maximizing the diversity of the local atomic environments surrounding the defect in terms of the atomic compositions in the first nearest neighbor shell. The total number of calculated sites for each dopant is around 50 for vacancies and 50 for interstitials. As we compare the effects of doping, the total number of calculations for four dopants and the pristine HEA is 250 for vacancies and 250 for interstitials. For migration cases, we consider one possible migration path for each of the defects considered. The total number of calculated migration barriers is then the same as the total number of formation energy calculations.

2.2. kMC simulations

To evaluate the impact of DFT-calculated defect energetic on atomic transport, kMC simulations were established where migration energies were drawn from DFT-informed defect distributions. Specifically, the migration energy distributions were fitted with Gaussian forms. At each kMC step, the energy barriers for all possible 1nn jumps were picked from the Gaussian distribution. Based on the barrier energies E_i, the transition rate for each possible jump was calculated by

$$\Gamma_i = \Gamma_0 \exp\left(-\frac{E_i}{k_B T}\right), \tag{4}$$

where $\Gamma_0 = 10$ THz was used for the attempted frequency, k_B is the Boltzmann constant, and T is the temperature. The total rate is $\Gamma_{tot} = \sum_i \Gamma_i$, based on which the time interval for the jump can be ob-

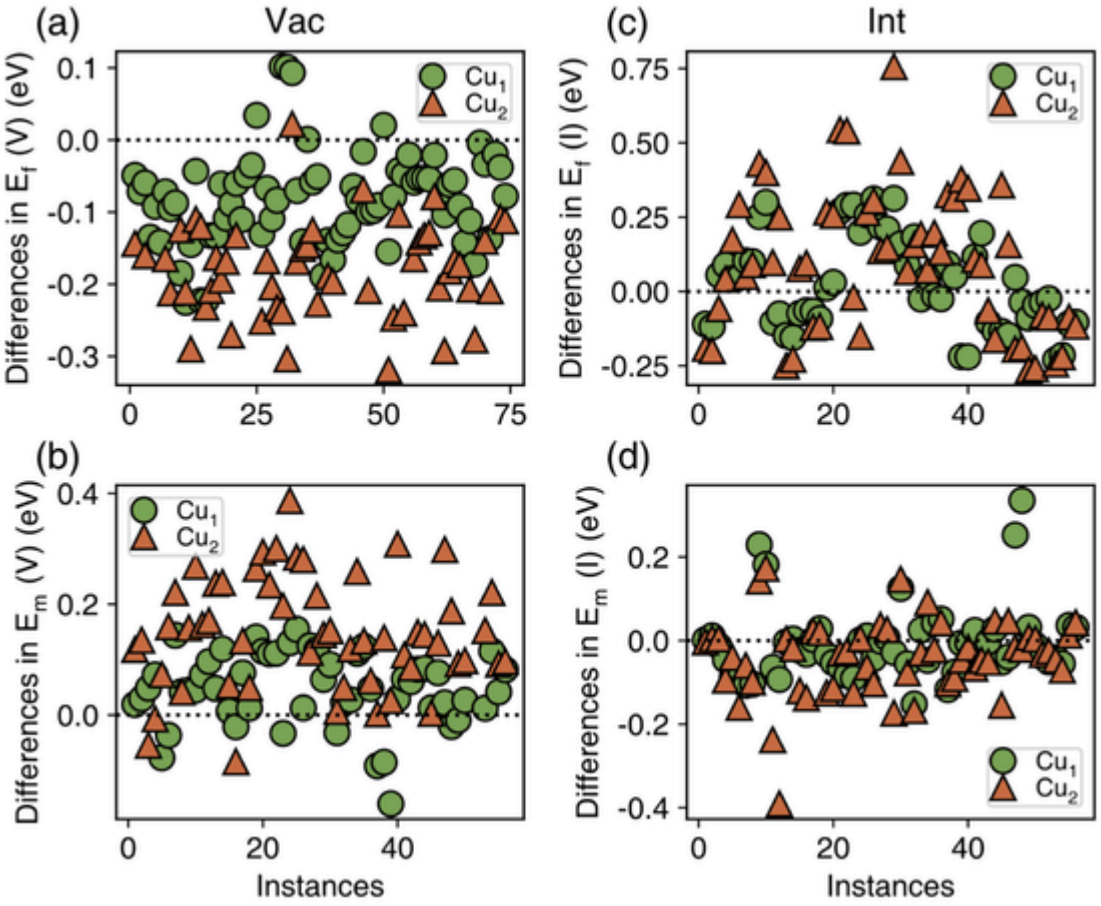

Fig. 5. Effects of increasing the concentration of Cu dopants in the 1nn shell around the defect on the differences of defect energies E_f(V), E_m(V), E_f(I), and E_m(I). All energies are shown with respect to those in the pristine CoCrFeNi.

Table 2
Influences of dopant concentration in the 1nn shell of the defects on defect energies. The values are given in eV.

	Al_1	Al_2	Cu_1	Cu_2
E_f(V)	-0.10	-0.15	-0.08	-0.18
E_m(V)	0.13	0.22	0.06	0.15
E_f(I)	-0.01	0.08	0.00	0.09
E_m(I)	-0.01	-0.02	-0.02	-0.04

tained through $\Delta t = \frac{1}{\Gamma_{tot}} \ln\left(\frac{1}{r}\right)$, where r is a random number in the range of (0,1]. The executed defect jump is chosen based on another random number, as in the standard kMC algorithm [45]. All simulations were performed in a 10 × 10 × 10 *fcc* supercell containing 4000 lattice sites. At each considered case, a total of 10^4 defect jumps were simulated. Periodic boundary conditions were employed in three dimensions.

From the obtained defect trajectory, the atomic square displacement (ASD) for all atoms can be calculated. The tracer diffusion coefficients D^* is then calculated from the time-ASD curve:

$$D^* = \frac{\langle R_i^2 \rangle}{2nt}, \tag{5}$$

where $\langle R_i^2 \rangle$ is ASD, t is time, and $n = 3$ is the dimensionality of defect diffusion considered in this study.

3. Result

Defect properties in pristine CoCrFeNi have been reported in our previous study [35]. It is well established that defect energetics in HEAs strongly depend on local atomic environments. Particularly, the most significant influences on point defect energetics come from the compositions in the 1nn shell around the defect. Therefore, to probe the effects of minor doping impurities, we compare defect properties before and after replacing one or two lattice atoms in the 1nn shell of the defect with desired dopant elements. Here substitutions of two lattice atoms are considered to investigate the effects of increasing dopant concentration and keep the overall dopant concentration at a dilute limit. One example is illustrated in Fig. 1, where the formation and migration of a [100] Cr-Cr interstitial dumbbell are shown. In this process, the initial and final states in (a) and (c) are both [100] dumbbells, while the configuration in (b) is the saddle structure. In this fig., two lattice atoms in the 1nn shell of the interstitial are replaced by two impurity atoms. The energies obtained before and after substitution are compared.

3.1. Influence of doping elements on defect energetics

The influences of doping elements on defect energies in CoCrFeNi are displayed in Fig. 2. For each defect type, the differences induced by the substitution, ΔE_f, are plotted. For vacancies, it is seen that all doping elements tend to decrease E_f(V) but increase E_m(V), though the magnitude varies depending on the doping element. Based on our calculations [35], the formation energy of vacancies decreases with increasing atomic number ($E_f(V_{Cr}) < E_f(V_{Fe}) < E_f(V_{Co}) < E_f(V_{Ni})$). This trend is in opposition to the trend of migration barriers for these vacancies. After

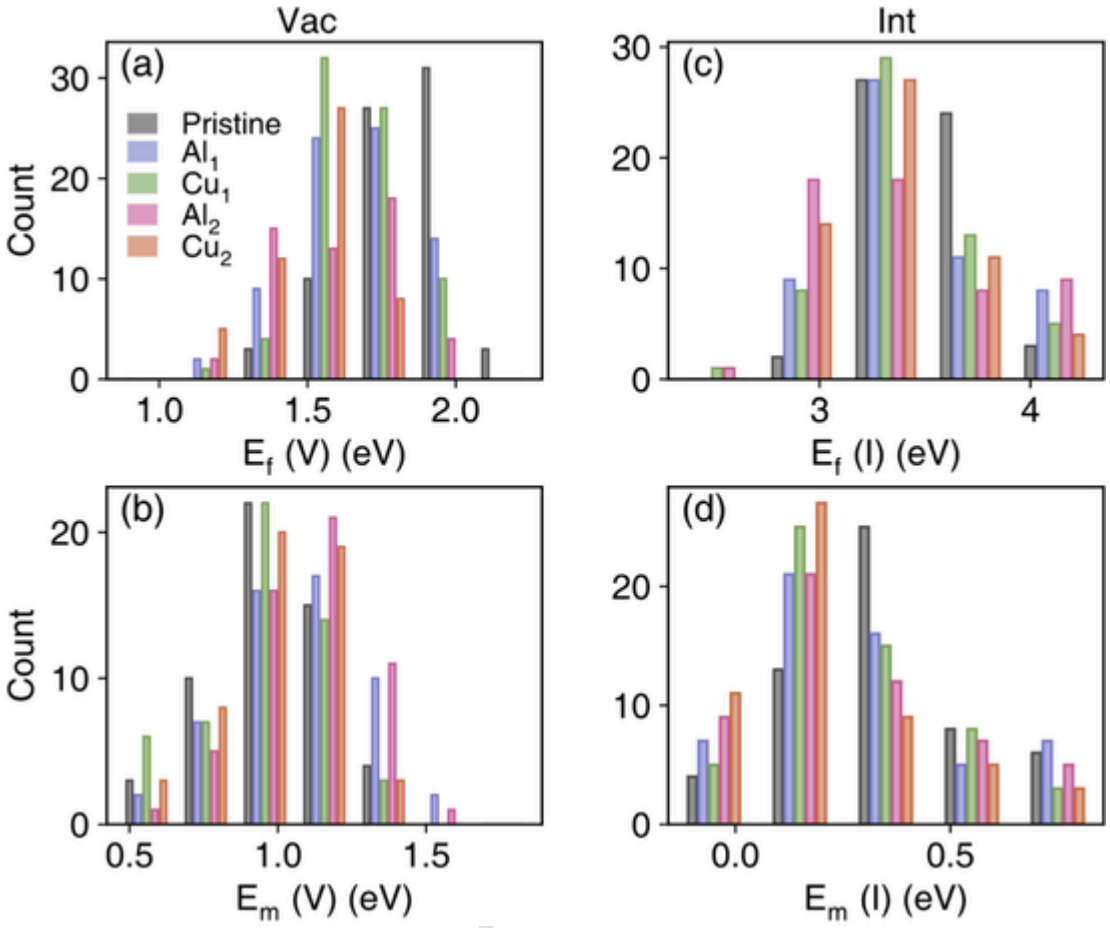

Fig. 6. Distribution of defect energies in pristine and doped CoCrFeNi with different concentrations of Al and Cu in the 1nn shell.

Table 3
Gaussian distribution parameters for the distributions of vacancy formation and migration energies (in eV).

	E_f(V)		E_m(V)	
	μ	σ	μ	σ
HEA	1.75	0.16	0.89	0.19
Al-doped HEA	1.67	0.18	1.03	0.19
Cu-doped HEA	1.66	0.17	0.96	0.18
Pd-doped HEA	1.57	0.17	1.13	0.19
Ti-doped HEA	1.59	0.19	1.23	0.21

doping, the effects on each type of vacancy are provided in the Supplement Material. We find that the impact of doping depends on vacancy types, where $E_f(V_{Cr})$ and $E_f(V_{Fe})$ are much more influenced than $E_f(V_{Co})$ and $E_f(V_{Ni})$. On the other hand, the differences in E_f(I) are spread around zero. For E_m(I), it is shown that doping elements can slightly decrease their migration energies. The averaged ΔE_f values are summarized in Table 1, which demonstrates the effects of different doping elements. In general, the most significant changes are found for the Ti dopant, which induces a notable increase in E_m(V) and a decrease in E_f(I) and E_f(V). The next most influential element is Pd. Based on the data in Table 1, the presence of Cu and Al in the 1nn shell of the defect have similar effects.

The overall distributions of defect energies in pristine CoCrFeNi and doped ones are demonstrated in Fig. 3. It is suggested that doping can broaden the defect energy distributions, especially for vacancies, i.e., E_f(V) and E_m(V). Therefore, doping is an effective way to tune the roughness of the defect energy landscape of HEAs. Fig. 3 also shows that the distribution of E_m(V) extends toward higher energies, especially for Ti-doped CoCrFeNi, indicating that vacancy migration is more likely to be suppressed due to the presence of Ti in the 1nn shell.

Previous studies imply that the overlap between distributions of E_m(V) and E_m(I) may be an important reason for the suppressed defect accumulation in HEAs [46]. In the doped CoCrFeNi here, we find that E_m(V) tends to be higher due to doping. On the other hand, Pd and Al lead to an increase of E_m(I). Comparing the distribution E_m(V) and E_m(I), it is therefore indicated that Pd and Al dopants may enhance the heterogeneity of defect motion, promoting defect recombination.

3.2. Effects of doping concentration

To examine the effects of doping concentration on defect energetics in CoCrFeNi, we have increased the number of doping elements from one to two in the 1nn shell around the defect. In *fcc* structures, two atoms (defect sites) in 1nn share four common nearest neighbors. Therefore, we introduce the two dopants randomly in these four sites, both being nearest neighbors to the defect considered. The doping elements of Al and Cu are considered in this case. The differences in E_f(V), E_m(V), E_f(I), and E_m(I) induced by different doping concentrations are displayed in Fig. 4 and Fig. 5 for Al and Cu impurities, respectively. Generally, for both the Al and Cu dopants, increasing the dopant concentration leads to decreased E_f (V) and increased E_m(V). Besides, Fig. 4 and Fig. 5 show that higher concentrations of Al and Cu tend to broaden the distribution of E_f(I), though the influence on E_m(I) is small.

The averaged values from all calculations are summarized in Table 2. The energy change shows a consistent dependence on the concentrations of Al and Cu. The most noticeable difference is that increasing Al concentration leads to a higher increase in E_m(V) than Cu. Therefore, Al

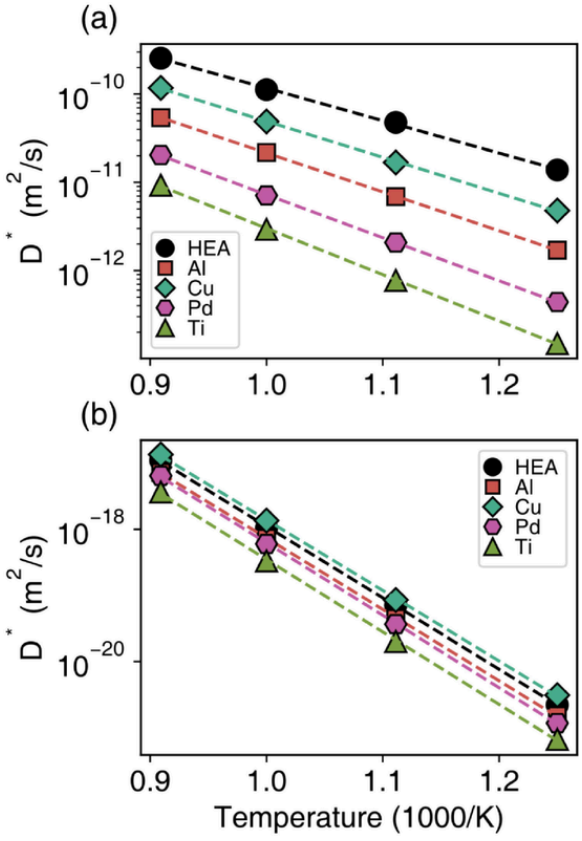

Fig. 7. Vacancy-mediated diffusion coefficients in pristine and doped CoCrFeNi HEA. (a) shows the results directly obtained from kMC simulations using the energy distribution in Table 3, (b) shows corrected diffusion coefficient by including the contributions from the prefactor from vacancy formation energies.

Table 4
Activation energies (E_a) and prefactor (D_0) deduced from the Arrhenius plot for diffusivity without and with considering the vacancy concentration (c_v).

	Without c_v		With c_v	
	E_a(eV)	D_0 (m²/s)	E_a(eV)	D_0 (m²/s)
HEA	0.73	5.63×10^{-7}	2.15	7.21×10^{-8}
Al	0.88	5.55×10^{-7}	2.14	4.67×10^{-8}
Cu	0.81	5.95×10^{-7}	2.12	6.61×10^{-8}
Pd	0.97	5.47×10^{-7}	2.18	5.72×10^{-8}
Ti	1.04	5.41×10^{-7}	2.18	3.21×10^{-8}

Table 5
Values of atomic radii and electronegativity for considered dopants [48,49]. For the CoCrFeNi HEA, the average and range are shown.

	Atomic size (Å)	Electronegativity
HEA	1.26 (1.25-1.28)	1.66 (1.56-1.75)
Al	1.43	1.47
Cu	1.28	1.75
Pd	1.38	1.35
Ti	1.46	1.32

doping exerts a stronger impact on vacancy diffusion properties in CoCrFeNi than Cu.

The overall energy distributions in pristine and doped CoCrFeNi are shown in Fig. 6. Increasing the dopant concentration leads to the appearance of more values in the lower and upper bounds, especially for E_f(V) and E_m(V). For instance, there is an increased fraction of E_m(V) at the lower bound around 0.5 eV after doping with Al_2 and Cu_2, which will stimulate vacancy diffusion significantly. Note that the changes in distribution are different from those of average values in Table 2. For HEAs, the distribution range of defect energies is more important since the migration of defects prefers the low energy portion of the distribution, as verified from our kMC simulations.

3.3. Diffusion results from kMC

The above results show that minor doping mainly changes the formation and migration energies of vacancies, whereas the influence on interstitial energetics is limited. Specifically, doping leads to a decrease in vacancy formation energies and an increase in migration energies. In addition to the changes in the mean values, the distribution width also shows variations. While the effects of increasing migration barriers are evident, it is not straightforward to assess the influence of varying distribution width. Therefore, we carry out kMC simulations to evaluate the effects.

For vacancy diffusion, the diffusion coefficients depend on both migration energies and formation energies as follows:

$$D^* = \Gamma_0 \lambda^2 f_{tr} \exp\left(-\frac{E_f}{k_B T}\right) \exp\left(-\frac{E_m}{k_B T}\right), \tag{6}$$

where λ is the jump distance and f_{tr} is the correlation factor. In HEAs, both E_f and E_m are widely distributed. By fitting the distributions to Gaussian formulae, we obtain the mean (μ) and standard deviation (σ) values, as provided in Table 3. Based on the distribution of migration energies, we draw E_m randomly for each step in kMC simulations. The obtained diffusion coefficients are displayed in Fig. 7(a). Consistent with the mean value of E_m(V) in Table 3, diffusivity is the highest in the pristine HEA, which also exhibits the lowest E_m(V). Doping leads to a decrease in diffusivities. The largest effect is found for Ti, in accordance with the highest E_m(V) in Table 3.

In kMC simulations, the effects of varying formation energies cannot be directly incorporated, which is related to the vacancy concentration c_v. To include the effects of E_f(V) distributions, we calculate the average of prefactor, i.e., $\left\langle \exp\left(-\frac{E_f}{k_B T}\right)\right\rangle$, where E_f follows a Gaussian distribution of $N\left(\mu_{E_f}, \sigma_{E_f}\right)$:

$$\left\langle \exp\left(-\frac{E_f}{k_B T}\right)\right\rangle = \exp\left(-\frac{\mu_{E_f}}{k_B T}\right) \exp\left(\frac{1}{2}\left(\frac{\sigma_{E_f}}{k_B T}\right)^2\right). \tag{7}$$

From this equation, it is seen that the distribution width σ_{E_0} will enhance the prefactor through the exponential term. Considering this effect, we normalize the calculated D^* from kMC by this factor. The corrected diffusivities are provided in Fig. 7(b). Compared to the results in Fig. 7(a), it indicates that E_f(V) can affect the diffusivities significantly. Particularly, the relative magnitude of diffusivities changes: Cu doping leads to a higher diffusivity, while Ti still exhibits the lowest diffusivity compared to the pristine HEA.

The activation energies can be deduced from the Arrhenius plot in Fig. 7 using

$$D^* = D_0 \exp\left(-\frac{E_a}{k_B T}\right). \tag{8}$$

The obtained values for E_a and D_0 are listed in Table 4. Without considering c_v, E_a reflects the dynamic average from E_m(V) distributions. It is found that in this case, E_a is lower than the mean values of E_m(V) distributions, suggesting that vacancy diffusion is biased towards lower energies with respect to the mean. With c_v considered, E_a contains the information from both E_m(V) and E_f(V) distributions. Similarly, we find that E_a is generally lower than the mean values of E_m(V) + E_f(V). There-

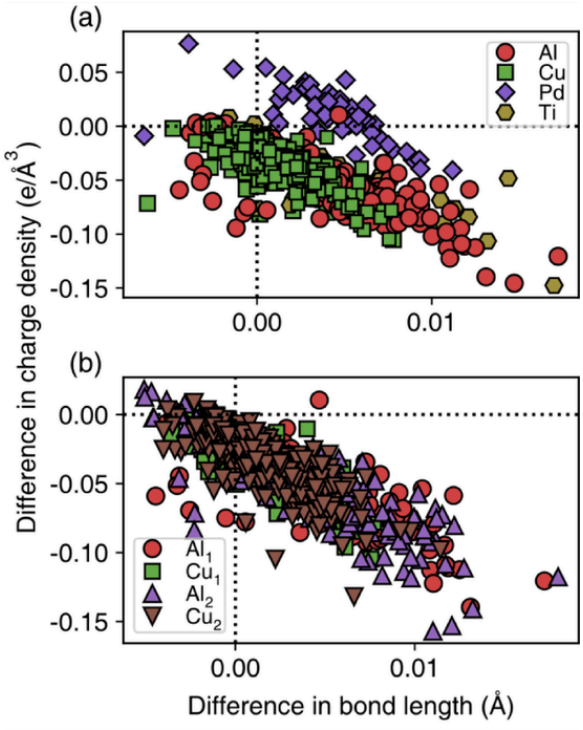

Fig. 8. The relationship between the changes of bond length in the 1nn shell and charge density in the bond center before and after dopant substitution. The results are collected from atoms in the 1nn shell surrounding the dopant in the perfect structure.

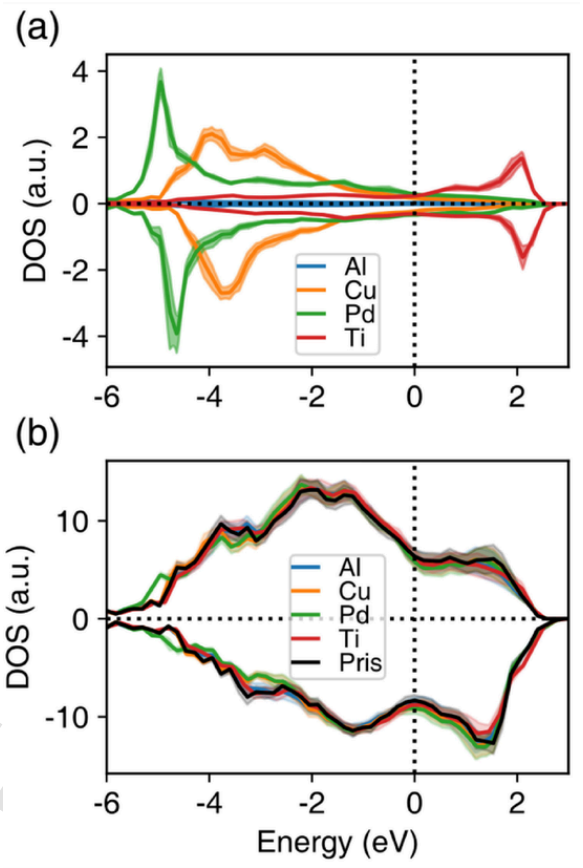

Fig. 9. The DOS for different dopant elements in CoCrFeNi (a) and DOS for the 12 lattice atoms in the 1nn shell bonding with the dopant.

fore, the energy distribution width plays a significant role in governing diffusion properties, as suggested in Eq. (7).

4. Discussion

4.1. Electronic origin of doping effects

The above results suggest that Ti and Pd generally exert larger influences on defect energetics in CoCrFeNi than Al and Cu (Ti > Pd > Al > Cu). Usually, in dilute alloys with trace impurities, the size misfit between the dopant and host is proposed as an important source of the impact. For instance, in pure Ni, it is found that the migration barriers in doped cases are governed by the size misfit between the dopant and Ni. As the size misfit increases, the energy barrier for the vacancy-Ni exchange increases [47]. The surmise in dilute alloys is first examined here for the studied CoCrFeNi HEA. The atomic radii of the four elements (Co, Cr, Fe, and Ni) are similar, with an average radius of 1.26 Å. The atomic radii for the four dopants considered here are listed in Table 5, which shows that the radius of the four elements is in the order of Cu < Pd < Al < Ti. Besides, it shows that the atomic radii of all these dopants (except for Cu), although maybe exhibiting variations in the CoCrFeNi HEA to adapt local chemical complexity, are larger than the HEA matrix, acting as oversized dopants in a simplified picture. From defect energies in Table 1, our results indicate that doping of Pd and Ti can enhance the vacancy migration barriers significantly than Al and Cu. Therefore, atomic size misfit can only partly explain the influence of considered dopants in this study. Specifically, our results for Cu and Ti dopants are consistent with the size misfit argument. Nonetheless, for Al with a larger size than Pd, we find that the effects of Al on defect energies are weaker than Pd with a smaller atomic size.

To further elucidate the impact induced by different dopants, we have calculated the changes of bond length in the 1nn shell before and after the introduction of the dopants. For each lattice atom, there are 12 nearest neighbors in the 1nn shell. The bond lengths of these 12 bonds are measured in the pristine HEA. After dopant substitution, the variations of these bond lengths (Δd_{bond}) are monitored. To exploit the electronic origin, we also calculated the charge density at each bond center before and after dopant substitution ($\Delta\rho$). The relationship between $\Delta\rho$ and Δd_{bond} is displayed in Fig. 8. It shows that a larger Δd_{bond} is usually associated with a more significant charge transfer $\Delta\rho$. There is a large portion of Δd_{bond} higher than 0, which is in line with the larger atomic size of these dopants. In particular, Ti and Al dopants can induce higher Δd_{bond} values compared to Cu and Pd. Among these four dopants, charge transfer surrounding Pd can be positive in most cases, contrary to others. For the other three elements, the magnitude of $\Delta\rho$ is in the order of Ti~Al > Cu, which is in accordance with the larger influence of Ti and Al on point defect energetics in Table 3. This trend is also consistent with the electronegativity of these elements as provided in Table 5, suggesting the dominant role of electronic interactions or electronic charge deformation flexibility [35].

In Fig. 8(b), the effects of increasing Al and Cu concentration are demonstrated. It suggests that higher Δd_{bond} values are found with higher concentrations of Al and Cu dopants, accompanying with more significant charge transfer $\Delta\rho$. The differences between Al and Cu are limited, though larger $\Delta\rho$ values are found for Al_2 than Cu_2. This could be the origin for the higher impact of Al_2 in influencing defect energies than Cu_2 as shown in Table 2.

The origin of charge transfer can be deduced from the density of states (DOS) for these dopants, as provided in Fig. 9(a). The shaded region denotes the average from different positions with variable local atomic environments. As Al only possesses *s* and *p* states, the DOS values are low compared to other dopants. For both Cu and Pd, the *d* orbitals are almost fully occupied, which is consistent with their electronic configurations ($3d^{10}$ and $4d^{10}$, respectively). On the other hand, the *d* orbitals of Ti are empty in both spin channels due to the low *d*

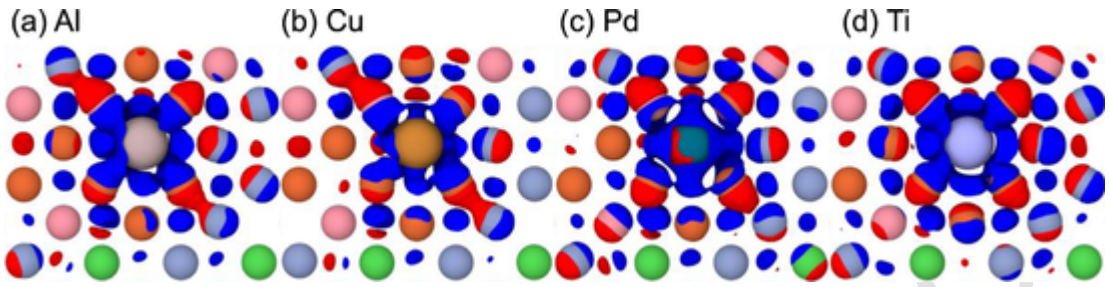

Fig. 10. Isosurface plot of charge density difference when a dopant is introduced into the CoCrFeNi HEA. The isovalue is set to be ± 0.03 e/Å^3, with the positive values denoted by the red color and negative by blue.

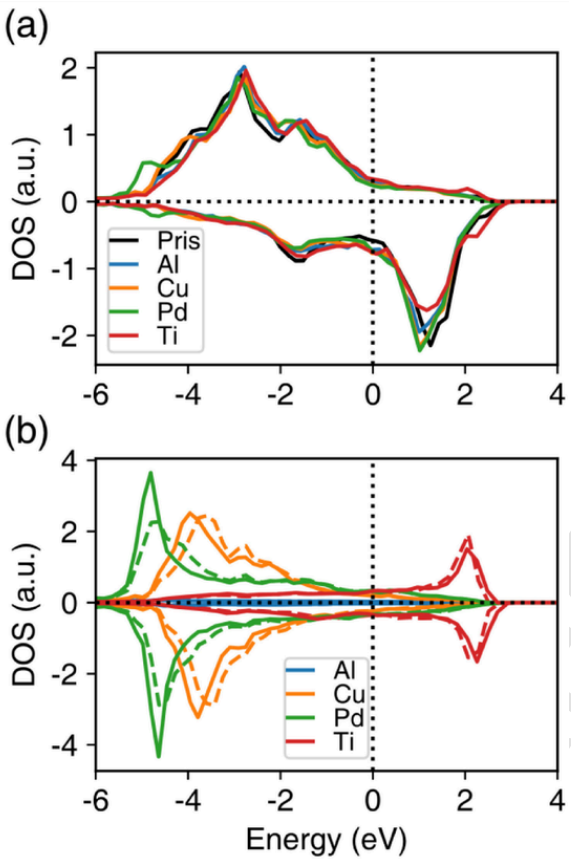

Fig. 11. (a) DOS for a Fe migrating atom in the saddle structure for a vacancy-Fe exchange, and (b) DOS of the dopants in the initial (dotted line) and saddle (solid line) configuration for the vacancy-Fe exchange event.

electron number. The unpaired electrons in Ti can form strong chemical bonds with surrounding lattice atoms, making lattice atom migration difficult and leading to higher migration energies for vacancy-lattice atom exchanges. For Pd, the DOS peaks are far away from the Fermi level, suggesting weak interactions between Pd and the elements in the HEA. This is the reason for the versatile charge transfer of Pd observed in Fig. 8.

The DOS of lattice atoms being the first nearest neighbors of the dopants before and after doping is displayed in Fig. 9(b). The DOS is averaged from different configurations; the spread is represented by the shaded region. The influence of the doping elements is small. Near the Fermi level, the DOS shapes can change markedly, especially for the Ti dopant, signifying the strong bonding interactions around Ti.

The charge density difference is further displayed in Fig. 10, which suggests charge loss surrounding the dopant element. Along with the [110] bonding direction, it can be seen that there is significant charge redistribution between Ti/Al and their neighbors, consistent with the quantitative analysis shown in Fig. 8. A comparison between Cu and Pd suggests that there are regions with positive isovalues surrounding Pd, leading to positive and negative $\Delta\rho$ as found in Fig. 8.

The differences in charge transfer in the bond region suggest a change in bond strength. For all the four dopants considered here, we find negative $\Delta\rho$ mostly, meaning charge loss, leading to weaker bonds. This is consistent with the lower vacancy formation energies in the doped HEAs. Specifically, weakened bonds make it easy to remove lattice atoms near the dopants. However, doping leads to higher migration barriers for vacancies. At the saddle structure, there is a lattice atom located at the center of the two nearest neighboring vacancies. We find that the distance between the dopant and the migrating atom is in the order of Pd > Ti > Al > Cu. Therefore, the migrating atom experiences larger compression in the saddle point for Pd and Ti, resulting in their higher energy barriers. A detailed analysis is exemplified in Fig. 11(a), where the DOS of a migrating Fe atom in the saddle structure of a vacancy-Fe exchange process is compared in the pristine and doped HEA. While the spin-up DOS exhibit minor changes after doping, the spin-down channel is filled by additional electrons, as evident by the increase of DOS near the Fermi level. The effect is more pronounced for Pd and Ti. Notably, the increase of DOS is the most significant for Ti-doped cases, leading to its highest energy barrier. In Fig. 11(b), we show the DOS of the dopants in the initial and transition states for a vacancy-Fe exchange event. For all dopants, the DOS peak shifts towards the lower-energy end with respect to the Fermi level, dictating increased electron occupation. In accordance with the DOS change of the migrating Fe, the largest occupation change is also found in Pd and Ti, suggesting the largest compression effects in the saddle structure in these two cases.

For interstitials, the influence of dopant elements on defect energies is less evident than vacancies due to the significant lattice distortion associated with interstitials. Therefore, we conclude that doping mainly influences vacancy-mediated transport properties in HEAs, such as solute diffusion.

To summarize, our results indicate that the influences of these dopants mainly come from both atomic size misfit and electronic charge deformation flexibility. For Cu with similar size and electronegative as the HEA, the effects on defect energetics are small. The interactions between Ti dopants with the HEA are the strongest due to their unoccupied electron states, leading to considerable charge transfer. For Pd, the DOS peak is away from the Fermi level, resulting in weak interactions with the HEA, though its large radius can exert compressive stress to surrounding lattice atoms. Finally, Al has no *d* electrons; its effects are mainly ascribed to size misfit and charge transfer from electronegativity differences.

4.2. Comparison with available results

The effects of minor impurities on defect properties have been extensively investigated in dilute alloys because of their important relevance for practical applications. However, in concentrated alloys, especially for HEAs, studies on dopant effects are extremely scarce, making

it difficult to compare our results with previous data. For pure metals, such as in pure Ni, the binding energy of Al, Cu, and Ti with vacancy at 1nn is 0.00, -0.03, and -0.05 eV, respectively. Our results obtained in the CoCrFeNi HEA are consistent with the results qualitatively [50]. However, our binding energies are more negative, suggesting that chemical disorder in the considered HEA enhances dopant-defect binding compared to pure metals.

Irradiation response of minor Al/Cu/Ti-doped CoCrFeNi HEA has been studied by Chen et al. [33]. It was found that He irradiation-induced bubbles usually exhibit a larger size, lower number density, and broader distribution range compared to the pristine HEA. Among the three dopants, the most pronounced influence is found in Ti. Our results here suggest that Ti doping indeed could enhance the heterogeneity of defect energy landscape in the pristine HEA, as evidenced by the highest σ in Table 3. This could be the reason for the broad distribution of experimentally observed bubble distributions.

The purpose of this study is to explore the influence of minor doping elements on defect properties in CoCrFeNi HEAs. To accentuate the effects of substitutional doping elements, we place the desired dopant elements into the 1nn shell around the defect, i.e., a vacancy or an interstitial dumbbell. A rough estimate of the doping concentration will be 1/12 as there are 12 atoms in the 1nn shell, giving rise to a concentration of 8.3%. In practice, the chance for the dopant element to reside in the 1nn shell of a defect is low at low doping concentrations. Therefore, our results intend to elucidate the effects of doping elements, but the concentrations may not be comparable to experiments. Besides, it has been well established that when the doping concentration is high, there may be phase instabilities in the CoCrFeNi HEA, such as at high Al/Cu/Ti concentrations [26,29,30,33]. Our results thus can be used to analyze the influence of doping at low concentrations without phase changes.

For HEAs, there is increasing evidence that short-range ordering (SRO) is an important feature of HEAs [51–53]. The presence of SRO will alter defect energetics and defect behavior since legal atomic environments around defects can be changed, and defect properties depend sensitively on the local environments, as revealed in this study. When SRO develops, available studies suggest that the defect process tends to be delayed due to the favorable bonding formation. Particularly, the local ordering regions may have stronger binding with defects, leading to a shift of defect energies so that defect dynamics may get retarded [54–56].

5. Conclusion

Based on first-principles calculations and kMC simulations, the influence of minor doping elements on the properties of defect energies is evaluated in a CoCrFeNi HEA. The effects of substitutional doping element species are investigated with Al, Cu, Pd, and Ti dopants bearing diverse valence electron configurations and atomic sizes, and different doping concentrations for Al and Cu are considered. Our results suggest that doping elements located at the 1nn shell of the defect exert a profound impact on defect energetics. Specifically, doping can decrease vacancy formation energies while enhancing migration energies at the same time. On the other hand, the energetics of interstitials are only slightly affected. Among the four elements, we find that Ti and Pd generally have more significant effects than Al and Cu in altering defect energies, which is attributed to the charge transfer and electronic interactions between the dopants and the constituent elements in HEAs. Increasing the doping concentration can further intensify the doping effects. Through kMC simulations with DFT energetics database, we show that doping can effectively tune atomic transport in HEAs. These results suggest that tunning the electronic properties of constitutive elements in a HEA matrix through doping with minor impurities is an effective strategy to manipulate defect energy landscape and improve irradiation resistance for HEAs.

Data availability

All data generated or analyzed during this study are included in this article.

CRediT authorship contribution statement

Shijun Zhao: Methodology, Investigation, Writing – original draft. **Yanwen Zhang:** Writing – review & editing. **William J. Weber:** Writing – review & editing, Writing – review & editing.

Declaration of Competing Interest

The authors declare that they have no known competing financial interests or personal relationships that could have appeared to influence the work reported in this paper.

Acknowledgment

This work was supported by the Research Grants Council of Hong Kong (No. 21200919). YZ and WJW were supported as part of Energy Dissipation to Defect Evolution (EDDE), an Energy Frontier Research Center funded by the U.S. Department of Energy, Office of Science, Basic Energy Sciences, under contract number DE-AC05-00OR22725.

Supplementary materials

Supplementary material associated with this article can be found, in the online version, at doi:10.1016/j.jnucmat.2022.153573.

Reference

[1] J.-W. Yeh, Physical metallurgy. High-Entropy Alloy, Springer International Publishing, Cham, 2016, pp. 51–113.
[2] D.B. Miracle, O.N. Senkov, A critical review of high entropy alloys and related concepts, Acta Mater. 122 (2017) 448–511.
[3] M.C. Gao, J.-W. Yeh, P.K. Liaw, Y. Zhang, High-Entropy Alloys, Springer International Publishing, Cham, 2016.
[4] J.W. Yeh, S.K. Chen, S.J. Lin, J.Y. Gan, T.S. Chin, T.T. Shun, C.H. Tsau, S.Y. Chang, Nanostructured high-entropy alloys with multiple principal elements: novel alloy design concepts and outcomes, Adv. Eng. Mater. 6 (2004) 299–303.
[5] B. Cantor, Multicomponent and high entropy alloys, Entropy. 16 (2014) 4749–4768.
[6] W.J.W.Y. Zhang, Y.N. Osetsky, Tunable chemical disorder in concentrated alloys: defect physics and radiation performance, Chem. Rev. (2021).
[7] M.-H. Tsai, J.-W. Yeh, High-entropy alloys: a critical review, Mater. Res. Lett. 2 (2014) 107–123.
[8] Y.F. Ye, Q. Wang, J. Lu, C.T. Liu, Y. Yang, High-entropy alloy: challenges and prospects, Mater. Today 19 (2016) 349–362.
[9] B. Gludovatz, A. Hohenwarter, K.V.S. Thurston, H. Bei, Z. Wu, E.P. George, R.O. Ritchie, Exceptional damage-tolerance of a medium-entropy alloy CrCoNi at cryogenic temperatures, Nat. Commun. 7 (2016) 10602.
[10] B. Gludovatz, A. Hohenwarter, D. Catoor, E.H. Chang, E.P. George, R.O. Ritchie, A fracture-resistant high-entropy alloy for cryogenic applications, Science 345 (2014) 1153–1158 (80-.).
[11] Y.Y. Chen, T. Duval, U.D. Hung, J.W. Yeh, H.C. Shih, Microstructure and electrochemical properties of high entropy alloys—a comparison with type-304 stainless steel, Corros. Sci. 47 (2005) 2257–2279.
[12] Y. Qiu, S. Thomas, M.A. Gibson, H.L. Fraser, N. Birbilis, Corrosion of high entropy alloys, Npj Mater. Degrad. 1 (2017) 15.
[13] Y. Zhang, S. Zhao, W.J. Weber, K. Nordlund, F. Granberg, F. Djurabekova, F. Granbergc, F. Djurabekova, Atomic-level heterogeneity and defect dynamics in concentrated solid-solution alloys, Curr. Opin. Solid State Mater. Sci. 21 (2017) 221–237.
[14] Y. Zhang, K. Jin, H. Xue, C. Lu, R.J. Olsen, L.K. Beland, M.W. Ullah, S. Zhao, H. Bei, D.S. Aidhy, G.D. Samolyuk, L. Wang, M. Caro, A. Caro, G.M. Stocks, B.C. Larson, I.M. Robertson, A.A. Correa, W.J. Weber, Influence of chemical disorder on energy dissipation and defect evolution in advanced alloys, J. Mater. Res. 31 (2016) 2363–2375.
[15] Y. Zhang, G.M. Stocks, K. Jin, C. Lu, H. Bei, B.C. Sales, L. Wang, L.K. Béland, R.E. Stoller, G.D. Samolyuk, M. Caro, A. Caro, W.J. Weber, Influence of chemical disorder on energy dissipation and defect evolution in concentrated solid solution alloys, Nat. Commun. 6 (2015) 8736.
[16] F. Granberg, K. Nordlund, M.W. Ullah, K. Jin, C. Lu, H. Bei, L.M. Wang, F. Djurabekova, W.J. Weber, Y. Zhang, Mechanism of radiation damage reduction in equiatomic multicomponent single phase alloys, Phys. Rev. Lett. 116 (2016)

135504.
[17] Y. Osetsky, A.V. Barashev, L.K. Béland, Z. Yao, K. Ferasat, Y. Zhang, Tunable chemical complexity to control atomic diffusion in alloys, Npj Comput. Mater. 6 (2020) 38.
[18] Y. Yang, Z. Li, W. Zhang, Y. Ma, Q. Xiong, W. Li, S. Chen, Z. Wu, Concentration of "mysterious solute" in CoCrFeNi high entropy alloy, Scr. Mater. 211 (2022) 114504.
[19] X. Li, Z. Li, Z. Wu, S. Zhao, W. Zhang, H. Bei, Y. Gao, Strengthening in Al-, Mo- or Ti-doped CoCrFeNi high entropy alloys: a parallel comparison, J. Mater. Sci. Technol. 94 (2021) 264–274.
[20] Y. Osetsky, A.V. Barashev, Y. Zhang, Sluggish, chemical bias and percolation phenomena in atomic transport by vacancy and interstitial diffusion in Ni Fe alloys, Curr. Opin. Solid State Mater. Sci. 25 (2021) 100961.
[21] C. Lu, L. Niu, N. Chen, K. Jin, T. Yang, P. Xiu, Y. Zhang, F. Gao, H. Bei, S. Shi, M.R. He, I.M. Robertson, W.J. Weber, L. Wang, Enhancing radiation tolerance by controlling defect mobility and migration pathways in multicomponent single-phase alloys, Nat. Commun. 7 (2016) 13564.
[22] M.R. He, S. Wang, S. Shi, K. Jin, H. Bei, K. Yasuda, S. Matsumura, K. Higashida, I.M. Robertson, Mechanisms of radiation-induced segregation in CrFeCoNi-based single-phase concentrated solid solution alloys, Acta Mater. 126 (2017) 182–193.
[23] C. Lu, T. Yang, K. Jin, N. Gao, P. Xiu, Y. Zhang, F. Gao, H. Bei, W.J. Weber, K. Sun, Y. Dong, L. Wang, Radiation-induced segregation on defect clusters in single-phase concentrated solid-solution alloys, Acta Mater. 127 (2017) 98–107.
[24] K. Jin, C. Lu, L.M. Wang, J. Qu, W.J. Weber, Y. Zhang, H. Bei, Effects of compositional complexity on the ion-irradiation induced swelling and hardening in Ni-containing equiatomic alloys, Scr. Mater. 119 (2016) 65–70.
[25] N.A.P.K. Kumar, C. Li, K.J. Leonard, H. Bei, S.J. Zinkle, Microstructural stability and mechanical behavior of FeNiMnCr high entropy alloy under ion irradiation, Acta Mater. 113 (2016) 230–244.
[26] S. Xia, M.C. Gao, T. Yang, P.K. Liaw, Y. Zhang, Phase stability and microstructures of high entropy alloys ion irradiated to high doses, J. Nucl. Mater. 480 (2016) 100–108.
[27] X.-X. Wang, L.-L. Niu, S. Wang, Energetics analysis of interstitial loops in single-phase concentrated solid-solution alloys, J. Nucl. Mater. 501 (2018) 94–103.
[28] S. Zhao, W.J. Weber, Y. Zhang, Unique challenges for modeling defect dynamics in concentrated solid-solution alloys, Jom 69 (2017) 2084–2091.
[29] S. qin Xia, Z. Wang, T. fei Yang, Y. Zhang, Irradiation behavior in high entropy alloys, J. Iron Steel Res. Int. 22 (2015) 879–884.
[30] S.Q. Xia, X. Yang, T.F. Yang, S. Liu, Y. Zhang, Irradiation resistance in AlxCoCrFeNi high entropy alloys, Jom 67 (2015) 2340–2344.
[31] T. Yang, S. Xia, S. Liu, C. Wang, S. Liu, Y. Fang, Y. Zhang, J. Xue, S. Yan, Y. Wang, Precipitation behavior of AlxCoCrFeNi high entropy alloys under ion irradiation, Sci. Rep. 6 (2016) 32146.
[32] D. Chen, Y. Tong, J. Wang, B. Han, Y.L. Zhao, F. He, J.J. Kai, Microstructural response of He + irradiated FeCoNiCrTi0.2 high-entropy alloy, J. Nucl. Mater. 510 (2018) 187–192.
[33] D. Chen, S. Zhao, J. Sun, P. Tai, Y. Sheng, G. Yeli, Y. Zhao, S. Liu, W. Lin, W. Kai, J.-J. Kai, Effects of minor alloying addition on He bubble formation in the irradiated FeCoNiCr-based high-entropy alloys, J. Nucl. Mater. 542 (2020) 152458.
[34] E. Lu, J. Zhao, I. Makkonen, K. Mizohata, Z. Li, M. Hua, F. Djurabekova, F. Tuomisto, Enhancement of vacancy diffusion by C and N interstitials in the equiatomic FeMnNiCoCr high entropy alloy, Acta Mater. 215 (2021) 117093.
[35] S. Zhao, T. Egami, G.M. Stocks, Y. Zhang, Effect of d electrons on defect properties in equiatomic NiCoCr and NiCoFeCr concentrated solid solution alloys, Phys. Rev. Mater. 2 (2018) 013602.
[36] Y. Zhang, X. Wang, Y.N. Osetsky, Y. Tong, R. Harrison, S.E. Donnelly, D. Chen, Y. Wang, H. Bei, B.C. Sales, K.L. More, P. Xiu, L. Wang, W.J. Weber, Effects of 3d electron configurations on helium bubble formation and void swelling in concentrated solid-solution alloys, Acta Mater. 181 (2019) 519–529.
[37] P.E. Blöchl, Projector augmented-wave method, Phys. Rev. B. 50 (1994) 17953.
[38] G. Kresse, J. Furthmüller, Efficiency of ab-initio total energy calculations for metals and semiconductors using a plane-wave basis set, Comput. Mater. Sci. 6 (1996) 15–50.
[39] J.P. Perdew, K. Burke, M. Ernzerhof, Generalized gradient approximation made simple, Phys. Rev. Lett. 77 (1996) 3865.
[40] J.M. Cowley, Short-range order and long-range order parameters, Phys. Rev. 138 (1965) A1384.
[41] J.M. Cowley, An approximate theory of order in alloys, Phys. Rev. 77 (1950) 669–675.
[42] S. Zhao, G.M. Stocks, Y. Zhang, Stacking fault energies of face-centered cubic concentrated solid solution alloys, Acta Mater. 134 (2017) 334–345.
[43] S. Zhao, G.M. Stocks, Y. Zhang, Defect energetics of concentrated solid-solution alloys from ab initio calculations: $Ni_{0.5}Co_{0.5}$, $Ni_{0.5}Fe_{0.5}$, $Ni_{0.8}Fe_{0.2}$ and $Ni_{0.8}Cr_{0.2}$, Phys. Chem. Chem. Phys. 18 (2016) 24043–24056.
[44] C. Domain, C.S. Becquart, Ab initio calculations of defects in Fe and dilute Fe-Cu alloys, Phys. Rev. B - Condens. Matter Mater. Phys. 65 (2002) 1–14.
[45] A.F. Voter, Introduction to the kinetic monte carlo method. Radiat. Eff. Solids, Springer, Netherlands, Dordrecht, 2007, pp. 1–23.
[46] S. Zhao, On the role of heterogeneity in concentrated solid-solution alloys in enhancing their irradiation resistance, J. Mater. Res. 35 (2020) 1103–1112.
[47] M. Krcmar, C. Fu, A. Janotti, R. Reed, Diffusion rates of 3d transition metal solutes in nickel by first-principles calculations, Acta Mater. 53 (2005) 2369–2376.
[48] C. Kittel, D.F. Holcomb, Introduction to Solid State Physics, Wiley, 1967.
[49] E.J. Little, M.M. Jones, A complete table of electronegativities, J. Chem. Educ. 37 (1960) 231.
[50] J.D. Tucker, Solute-vacancy interactions in nickel, MRS Proc. 1645 (2014), mrsf13-1645-ee08-08.
[51] R. Zhang, S. Zhao, J. Ding, Y. Chong, T. Jia, C. Ophus, M. Asta, R.O. Ritchie, A.M. Minor, Short-range order and its impact on the CrCoNi medium-entropy alloy, Nature 581 (2020) 283–287.
[52] S. Chen, Z.H. Aitken, S. Pattamatta, Z. Wu, Z.G. Yu, D.J. Srolovitz, P.K. Liaw, Y.-W. Zhang, Simultaneously enhancing the ultimate strength and ductility of high-entropy alloys via short-range ordering, Nat. Commun. 12 (2021) 4953.
[53] V. Sorkin, S. Chen, T.L. Tan, Z.G. Yu, M. Man, Y.W. Zhang, First-principles-based high-throughput computation for high entropy alloys with short range order, J. Alloys Compd. 882 (2021) 160776.
[54] S. Zhao, Effects of local elemental ordering on defect-grain boundary interactions in high-entropy alloys, J. Alloys Compd. 887 (2021) 161314.
[55] S. Zhao, Role of chemical disorder and local ordering on defect evolution in high-entropy alloys, Phys. Rev. Mater. 5 (2021) 103604.
[56] J. Ding, Q. Yu, M. Asta, R.O. Ritchie, Tunable stacking fault energies by tailoring local chemical order in CrCoNi medium-entropy alloys, Proc. Natl. Acad. Sci. U. S. A. 115 (2018) 8919–8924.